Fermi National Accelerator Laboratory

FERMILAB-Conf-83/56-EXP
7340.203
LBL-16286

MEASUREMENT OF THE NUCLEON STRUCTURE FUNCTION IN IRON USING 215 AND 93 GeV MUONS*

A. R. Clark, K. J. Johnson, L. T. Kerth, S. C. Loken, T. W. Markiewicz, P. D. Meyers, W. H. Smith, M. Strovink, and W. A. Wenzel
Physics Department and Lawrence Berkeley Laboratory
University of California, Berkeley, California 94720

and

R. P. Johnson, C. Moore, M. Mugge, and R. E. Shafer
Fermi National Accelerator Laboratory, Batavia, Illinois 60510

and

G. D. Gollin, F. C. Shoemaker, and P. Surko
Joseph Henry Laboratories, Princeton University, Princeton, New Jersey 08544

August 1983

*Contributed to the 1983 International Symposium on Lepton and Photon Interactions at High Energies, Cornell University, Ithaca, New York 14853, August 4-9, 1983.

Operated by Universities Research Association Inc. under contract with the United States Department of Energy

FERMILAB-Conf-83/56-EXP
7340.203
LBL-16286

Measurement of the Nucleon Structure Function in Iron Using 215 and 93 GeV Muons

A.R. Clark, K.J. Johnson,[a] L.T. Kerth, S.C. Loken, T.W. Markiewicz,[b]
P.D. Meyers, W.H. Smith,[c] M. Strovink, and W.A. Wenzel

Physics Department and Lawrence Berkeley Laboratory
University of California, Berkeley, California 94720

R.P. Johnson, C. Moore, M. Mugge, and R.E. Shafer

Fermi National Accelerator Laboratory
Batavia, Illinois 60510

G.D. Gollin[d], F.C. Shoemaker, and P. Surko[e]

Joseph Henry Laboratories, Princeton University
Princeton, New Jersey 08544

Abstract

We present measurements of the nucleon structure function $F_2(x,Q^2)$. The measurements are based on deep inelastic scattering of 215 and 93 GeV muons incident on the solid iron Multimuon Spectrometer at Fermilab. Using a lowest-order QCD calculation we find a best-fit value of $\Lambda_{LO} = 230 \pm 40^{stat} \pm 80^{syst}$.

Using the deep inelastic scattering of high energy muons, we have measured the structure function of nucleons in iron. Neglecting the muon and nucleon masses, the lowest order QED cross section for inelastic muon-nucleon scattering is

$$\frac{d^2\sigma}{dQ^2dx} = \frac{4\pi\alpha^2}{Q^4} \left(1-y+\frac{1}{2(R+1)}\ y^2\right) F_2\ (x,Q^2)/x \qquad (1)$$

Here Q^2 is the square of the muon 4-momentum transfer, $x \equiv Q^2/2M_N\nu$, $y \equiv \nu/E$, and $\nu \equiv E-E'$ is the energy lost by the muon. $R \equiv \sigma_L/\sigma_T$ is the ratio of cross sections for longitudinally and transversely polarized virtual photons and is expected to be small. In the parton model, x represents the fraction of the target nucleon momentum carried by the struck parton, and the structure function F_2, a function of x only, represents the momentum distribution of partons in a nucleon. This picture remains useful in quantum chromodynamics (QCD), but interactions among partons (now quarks and gluons) are expected to introduce Q^2 dependence to F_2.

The measurements presented here are drawn from data taken using the Multimuon Spectrometer (MMS, Fig. 1) in the muon beam at Fermilab. In the experiment, beams of 215 and 93 GeV muons penetrated 91 four-inch thick iron plates, which provided a 5.3 kg/cm^2 target, a 20 kG magnetic field for momentum analysis, a hadron absorber, and a hadron calorimetry medium. Large rectangular trigger counters were located at 10-plate (178 cm) intervals above and below the beam. The inside edges of the upper and lower counters were 54 cm apart, with the intervening region used as a beam veto. The trigger demanded a single beam muon entering the MMS and hits in any three consecutive trigger counters, with no hits in the corresponding beam vetoes. No hadron energy deposition requirement was made. Taking into account the large (20 cm) beam size, the minimum vertical scattering angle accepted was approximately 12 mrad. Muon

trajectories were measured with multiwire proportional chambers and drift chambers located after every fifth plate. Hadron shower energies were measured calorimetrically using pulse heights in plastic scintillators located after every plate.

This analysis is based on 8×10^5 (6×10^4) deep inelastic triggers from 2.4×10^{11} (8×10^9) muons of 215 (93) GeV incident energy. The beam flux is determined by directly counting the incident muons during the live intervals of the experiment. Almost all of the triggered events are real deep inelastic scatters. The primary background comes from the loss of a beam muon due to decay or energy loss early in the MMS, accompanied by a second muon entering downstream through the top or the bottom. These events are rejected in analysis by requiring an intersection of the beam and scattered tracks.

Scattered tracks are found at the back of the spectrometer and followed up to a tentative interaction point determined from calorimeter counter pulse heights. Beam track finding is begun in proportional chambers located upstream of the MMS and extended downstream to the interaction point. We then fit the momenta of the incident and scattered muons. Because the muons are travelling in essentially solid iron, the momentum fit allows for multiple scattering between each of the chambers. Finally, we require that the beam and scattered tracks be consistent with a common interaction vertex. In those events with a reconstructed beam track, we find the scattered track with >99% efficiency and successfully fit the event with 95% efficiency.

The average momentum resolution for scattered tracks in the MMS is $\sigma_{p'}/p'=8.6\%$ (9.0% for the 93 GeV data). At large E', we improve the ν and x resolution by using the direct calorimetric measurement of ν with resolution $\sigma_\nu/\nu=1.4[\nu\ (\mathrm{GeV})]^{-\frac{1}{2}}$.

The acceptance of the MMS is determined using a Monte Carlo calculation. This calculation is used also to correct for resolution smearing, radiative effects (including highly non-Gaussian tails from large energy losses), and inefficiencies of chambers and trigger counters. The simulation starts with an unbiased sample of real beam tracks and propagates each to a randomly chosen vertex allowing for dE/dx and multiple scattering in each plate. At the vertex, an outgoing muon is generated using the radiatively corrected[1] deep inelastic cross section with R=0 and an initial guess for F_2 (x,Q^2) based on older experiments.[2,3] This muon is propagated further and the trajectory is checked to see if the trigger is satisfied. Simulated events that satisfy the trigger are recorded in the same format used for the raw data with an additional block containing the true kinematics of the event. The Monte Carlo-generated events are then treated like data by the analysis programs.

Before extracting F_2 (x,Q^2) from the data, we apply several cuts to both real and simulated events. First, for the 215 (93) GeV samples, a cut of $Q^2 >$ 10 (4) GeV^2/c^2 is applied because the simulation was carried out only above a Q^2 of 6 (2.6) GeV^2/c^2. Next it is demanded that there be one and only one scattered track and that the reconstructed track be consistent with the recorded pattern of hit counters that triggered the event. Finally a minimum ν of 20 (10) GeV, a minimum E' of 10 (10) GeV, and a missing energy of less than 96 (48) GeV are required. These last cuts remove 10-15% of both the real and simulated data. The regions removed are populated by the extreme tails of the resolution and energy loss distributions. Large missing energy indicates a catastrophic energy loss before scattering. In this case the events are badly misanalyzed. Catastrophic effects were included in our simulation as completely as possible before cuts were made.

The Monte Carlo simulation provides the absolute normalization of the data. Deficiencies in the simulation are revealed by different losses due to analysis failures and cuts in the real and simulated samples. This necessitates small corrections to the normalization which are +2.0% (+2.8%) for the 215 (93) GeV samples. The systematic uncertainly in the normalization for each sample is estimated to be 3% with a 2.5% relative uncertainty between the samples. Because the simulation is absolutely normalized, we can write

$$F_2^{meas}(x,Q^2) = \frac{cD(x,Q^2)}{M(x,Q^2)} F_2^{model}(x,Q^2) \qquad (2)$$

where c is the normalization correction, D and M are the number of real and simulated events, respectively, and F_2^{model} is the structure function used in the simulation. This method is equivalent to regarding the simulation simply as a calculation of the acceptance of the apparatus. It further takes radiative corrections (and all other effects modeled in the simulation) into account automatically and allows correction for resolution smearing effects.

The rapidly varying cross section and the poor x resolution, especially at low ν, make this resolution correction essential. This is illustrated in Fig. 2 where the knowledge of the true kinematics of Monte Carlo-generated events is used to show the average value of x_{true} for bins of $x_{measured}$. From this plot one can easily determine where data points will and will not appear in our final F_2 plots. For example, we cannot determine F_2 at $Q^2 = 128$ GeV$^2/c^2$, $x = 0.75$, even though we have hundreds of events with (unsmeared) Q^2 and x in this bin and the acceptance of the MMS in this region is at its maximum of 40%.[4] The resolution-induced feed down from the more populous low x region makes it impossible to isolate a subset of the data at this Q^2 with an average true x of 0.75. Using (2), we can allow for this feed down by binning data and Monte Carlo events in the same bins of measured x and Q^2, and then referring the

resulting F_2 to the average true x and Q^2 using the information illustrated in Fig. 2. When more than one bin produces data with nearly the same average true x and Q^2, the data are averaged after fitting.

The presence of F_2^{model} in (2) suggests that the F_2^{meas} yielded by this procedure is model dependent. Considering the simulation as merely an acceptance calculation or noting that in (2) $M(x,Q^2)$ is proportional to $F_2^{model}(x,Q^2)$, demonstrates that, to first order, this is not the case. However, changing the model sufficiently could change the shapes of distributions enough to affect the smearing or the distribution of events within finite sized bins. We remove this model dependence by empirically fitting F_2^{meas} and using this as the F_2^{model} for a next iteration. The signals that the iteration has converged are 1) stability against further change, and 2) identical distributions of data and simulation in many variables. In practice, one iteration satisfies both requirements.

The resulting measurements of F_2 (x,Q^2) for nucleons in iron are shown separately for the two beam energies in Fig. 3. The values have been interpolated to the true x and Q^2 indicated and are thus not bin averages. R is assumed to be zero, and no Fermi motion correction has been applied. The errors are statistical . We have eliminated points in three categories: 1) those with statistical uncertainty greater than 40%, 2) those from regions with acceptance less than 1/10 of the maximum, and 3) those with a contribution of greater than 90% from other bins via smearing. The results are not sensitive to the exact values of these cuts. Systematic errors can result from uncertainties in beam energy and magnetic field calibration, trigger counter efficiency, resolution modeling, and so on. As these effects cause correlated shifts in the measured points, we do not attach individual systematic error bars to points, but present instead the global effects of these systematic uncertainties on our fitted

results.

We have fit the F_2 measurements of Fig. 3 using a program originally supplied by R. Barnett.[5] The program incorporates the predictions of lowest order QCD as embodied in the Altarelli-Parisi evolution equations.[6] Starting with a parameterization of the x dependence of F_2 at a reference $Q^2 = Q_0^2$, the program integrates the evolution equations to generate predicted values of F_2 for all Q^2. These are compared to the measured values and adjustments are made to the Q_0^2 parameterization and to the QCD scale parameter Λ to minimize the discrepancies between measurement and prediction. The form of the parameterization we use is shown in Table I. Because our iron target is (nearly) a flavor singlet, as is the gluon, there is coupling between the evolution of the quark structure function which is directly measurable in this electromagnetic scattering experiment, and the distribution of gluons which is not. Neutrino experiments probe the gluons less indirectly and we use their results as a guide.[7] However, significant uncertainty in the gluon sector remains and this results in considerable uncertainty in Λ.[8]

The result of the fit is shown in Fig. 3 and as entry (a) of Table I. The errors listed in the table are statistical only. Other contributions to the uncertainty in Λ are systematic experimental effects and the phenomenological uncertainties mentioned above. In fit (b) the normalization of the 93 GeV sample is allowed to vary with respect to the fixed normalization of the 215 GeV sample. This procedure reduces the 93 GeV sample normalization by 2%, consistent with the uncertainty in the relative normalization. Systematic uncertainties in Λ from this source and others are compiled in Table II. Also shown in Table I are the effects of plausible variations in the parameterization used in the fit. Fit (c) shows the (small) effect of changing the form of the parameterization. In fits (d) and (e) the assumed values of some of the

otherwise fixed parameters in the fit are changed. Fit (e) in particular shows the sensitivity of Λ to the "hardness" of the assumed gluon momentum distribution.

We also determine the effect on Λ of changing some of our analysis assumptions. If instead of R=0 we assume R=0.1, Λ decreases by 100 MeV/c. Applying a correction for Fermi motion using the method of West[9] and of Bodek and Ritchie[10] changes Λ by from +20 to +70 MeV/c. From Ref. (8) we estimate the effect of a next-to-leading-order QCD calculation to be on the order of +50 MeV/c. Changing Q_0^2 to 25 GeV^2/c^2 has no effect on Λ.

Figure 4 shows a comparison of our results, averaged over the beam energies, with those of the European Muon Collaboration's (EMC's) iron target experiments.[11] For purposes of this comparison only, our data have been multiplied by a factor of 0.953. Both data sets are uncorrected for Fermi motion and assume R=0. Table I includes an entry for a fit to EMC's data using our fitting routine and assumptions. These fitted parameters are consistent with EMC's published results[12] although the assumptions made here are slightly different. The EMC also has reported differences of up to 15% between deuterium and iron in the x dependence of F_2 that are not explained by Fermi motion.[13,14] Of course, our experiment uses only an iron target. In Figure 5 we show the ratio of our F_2(Fe) (multiplied by 0.953) to that of EMC, for $Q^2 > 50$ GeV^2/c^2. The errors are statistical; systematic uncertainties are approximately the same in magnitude. Also shown is the rough trend of EMC's $F_2(d)/F_2(Fe)$. Our data is clearly in better agreement with EMC's iron data than with their deuterium data.

To summarize, we have made a high statistics measurement of the structure function of nucleons in iron over the range $5 < Q^2 < 200$ GeV^2/c^2. We find scaling violations as suggested by QCD and find a value of $\Lambda = 230 \pm 40^{stat} \pm 80^{syst}$ Mev/c where systematic and phenomenological uncertainties dominate.

References

a. Now at University of Notre Dame, Department of Physics, Notre Dame, IN 46556.

b. Now at CERN, CH-1211, Geneva 23, Switzerland.

c. Now at Nevis Laboratories, P.O. Box 137, Irvington, NY 10533.

d. Now at Enrico Fermi Institute, Chicago, IL 60637.

e. Now at Bell Laboratories, Murray Hill, NJ 07974.

1. L.W. Mo and Y.S. Tsai, Rev. Mod. Phys. 41, 205 (1969).

2. E.M. Riordan et al., SLAC-Pub-1634 (1975).

3. A.J. Buras and K.J.F. Gaemers, Nucl. Phys. B132, 249, (1978).

4. The maximum acceptance is less than 100% because of the minimum vertical scatter required by the trigger.

5. L.F. Abbott, W.B. Atwood, and R. Michael Barnett, Phys. Rev. D22, 582 (1980).

6. G. Altarelli and G. Parisi, Nucl. Phys. B126, 298 (1977).

7. H. Abramowicz et al., Z. Phys. C12, 289 (1982).

8. A. Devoto, D.W. Duke, J.F. Owens, and R.G. Roberts, Phys. Rev. D27, 508 (1983).

9. G.B. West, Ann. Phys. (N.Y.) 74, 464 (1972).

10. A. Bodek and J.L. Ritchie, Phys. Rev. D23, 1070 (1981).

11. J.J. Aubert et al., Phys. Lett. 105B, 322 (1981).

12. J.J. Aubert et al., CERN-EP/82-48, 29 April 1982.

13. J.J. Aubert et al., Phys. Lett. 123B, 275 (1983).

14. A. Bodek et al., Phys. Rev. Lett. 50, 1431 (1983).

Table I. Results of lowest-order QCD fits to $F_2(x,Q^2)$. $F_2(x,Q_0^2)=Ax^{\alpha}(1-x)^{\beta}(1+ax)+B(1-x)^{\gamma}$; $G(x,Q_0^2)=C(1-x)^{\delta}$; a, γ, δ fixed; C from momentum sum rule; fit α, β, A, B, and Λ. Errors are statistical.

Fit	Λ(MeV/c)	α	β	A	B	a	χ^2/DOF	
a. Standard: γ=8, δ=5, a=0	225±43	1.00 ±0.10	3.80 ±0.15	2.74 ±0.44	0.410 ±0.036	...	156/94	Q_0^2=5.535 GeV^2/c^2
b. Fit 93 GeV norm.	176±43	0.99 ±0.10	3.83 ±0.15	2.67 ±0.43	0.409 ±0.035	...	150/93	norm. lowered by 2%
c. Fit a	225±43	0.51	3.97	0.84	0.948	3.24	155/93	
		(parameters are highly correlated)						
d. γ≡12	230±44	0.71 ±0.07	3.56 ±0.13	1.92 ±0.25	0.350 ±0.048	...	155/94	
e. δ≡6	201±40	1.00 ±0.10	3.83 ±0.14	2.77 ±0.44	0.408 ±0.036	...	154/94	
f. Standard, EMC data (Reference 11)	159±25	0.65 ±0.05	3.29 ±0.07	1.41 ±0.12	0.258 ±0.022	...	230/153	Q_0^2=5.50 GeV^2/c^2

Table II
Systematic Uncertainties in Λ

Source	Uncertainty (%)	Effect on Λ (MeV/c)
MMS B-field calibration	0.5	<10
Beam energy	0.5	15
Trigger efficiency (systematic)	0.5	16
Trigger efficiency (statistical)		10
Resolution smearing		50
93/215 GeV relative normalization	2.5	60
Total		82

Figure Captions

Figure 1. The Multimuon Spectrometer. Modules consist of 5 four-inch iron plates with interleaved instrumentation. S1, 2, 11, 12 = trigger counters; S3-10 = beam veto; PC, DC = tracking chambers; C = calorimeter counters.

Figure 2. Resolution smearing effects in x at 215 GeV.

Figure 3. F_2 (x,Q^2) for nucleons in iron. The Q^2 dependence is displayed for various fixed values of x. 93 GeV and 215 GeV data are shown separately. Errors are statistical only. The curves represent the lowest order QCD fit of entry (a) in Table I.

Figure 4. A comparison of our measurement of F_2 (x,Q^2) with EMC's iron target measurement (reference 11). Our F_2 has been multiplied by 0.953 for this comparison.

Figure 5. The ratio of our F_2 (Fe) to EMC's as a function of x for $Q^2 > 50$. Our F_2 has been multiplied by 0.953. The line shows the rough trend of EMC's F_2 (deuterium)/F_2 (Fe). (Reference 13.)

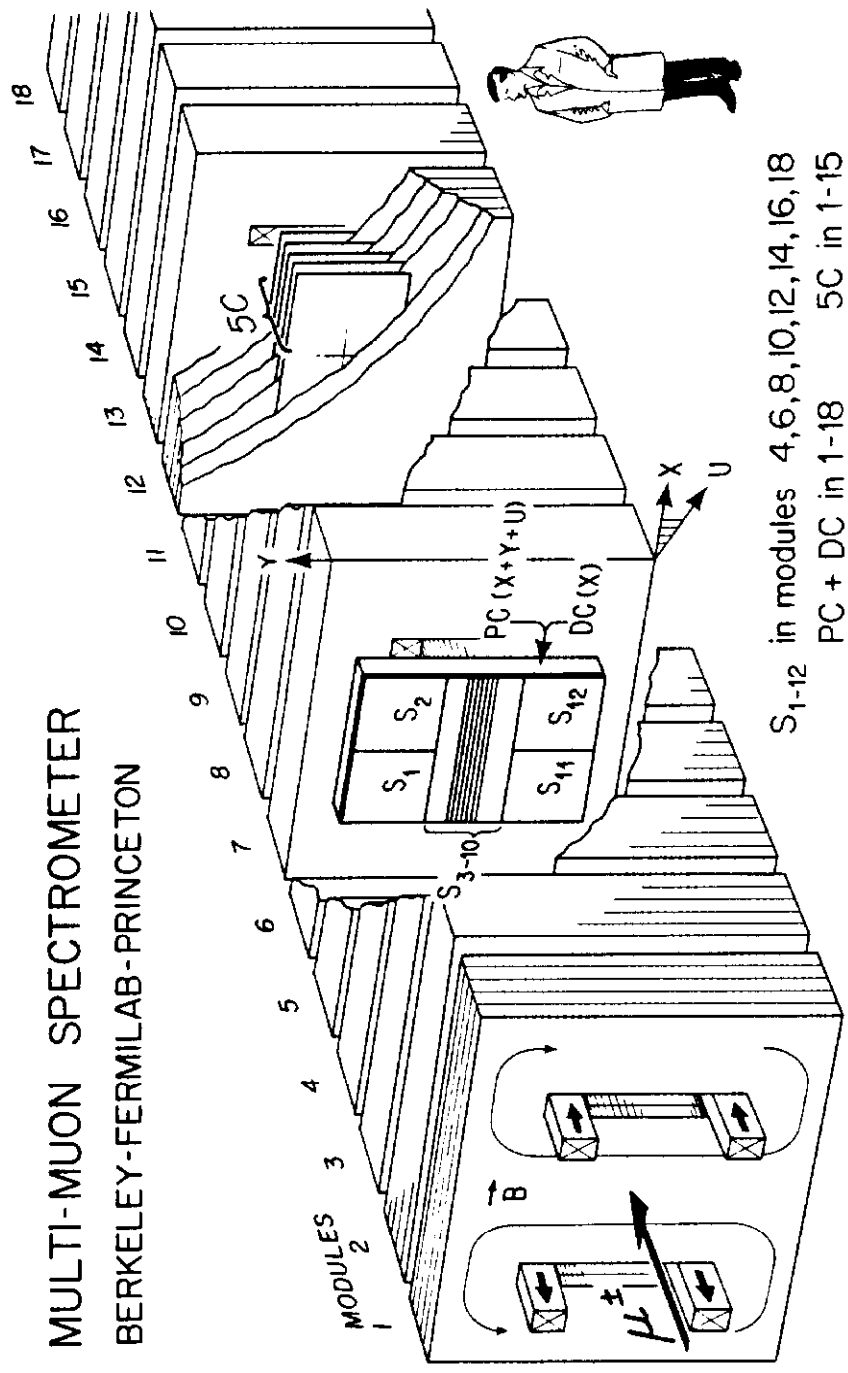
MULTI-MUON SPECTROMETER
BERKELEY-FERMILAB-PRINCETON
MODULES
1
2
3
4
5
6
7
8
9
10
11
12
13
14
15
16
17
18
5C
B
μ±
Y
X
U
PC (X+Y+U)
DC (X)
S1
S2
S11
S12
S3-10
S1-12 in modules 4,6,8,10,12,14,16,18
PC + DC in 1-18
5C in 1-15
XBL 795-9605

FIGURE 1.

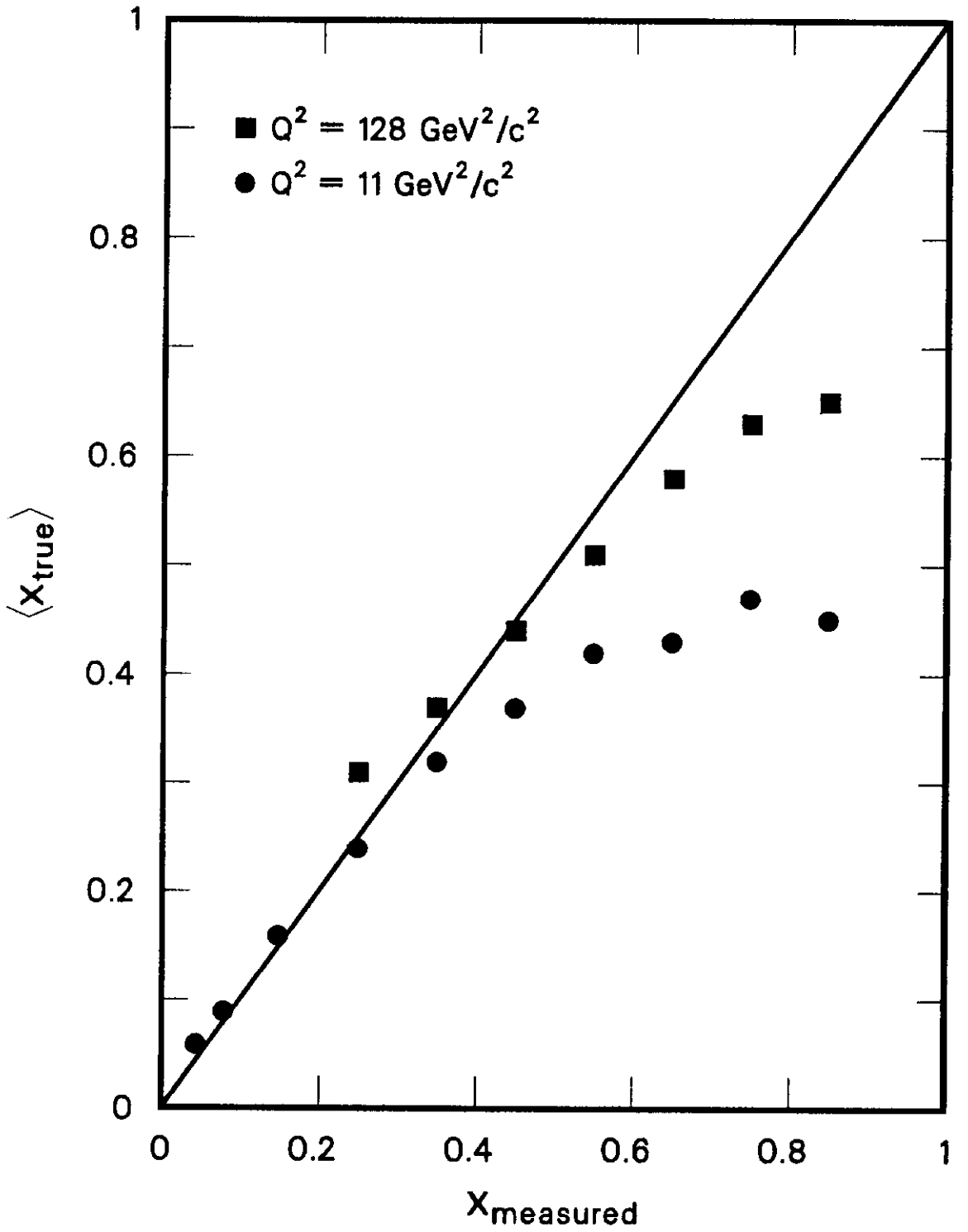

FIGURE 2.

XCG 836-7165

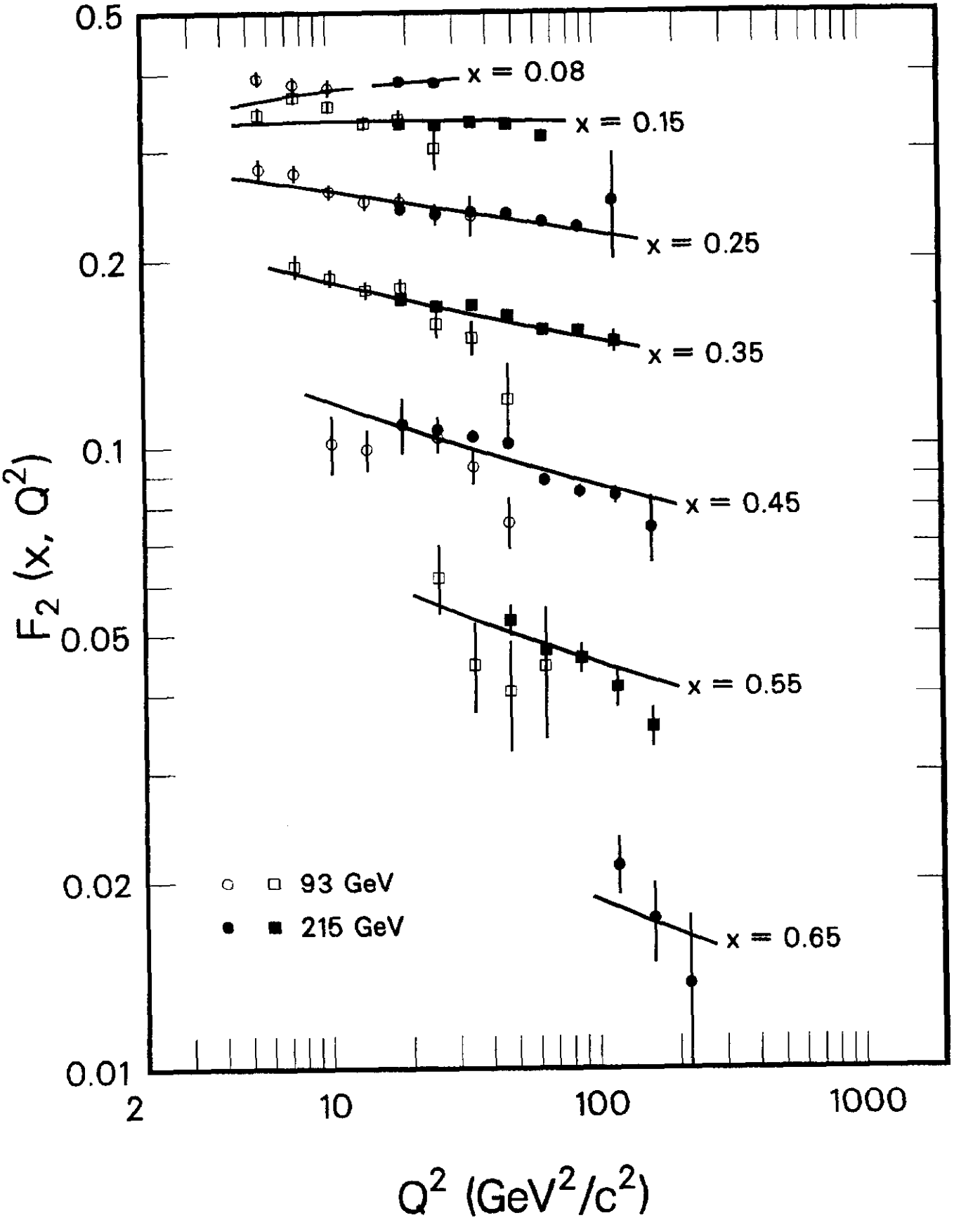
0.5
0.2
0.1
0.05
0.02
0.01
2
10
100
1000
$F_2(x, Q^2)$
Q^2 (GeV^2/c^2)
x = 0.08
x = 0.15
x = 0.25
x = 0.35
x = 0.45
x = 0.55
x = 0.65
93 GeV
215 GeV

FIGURE 3.

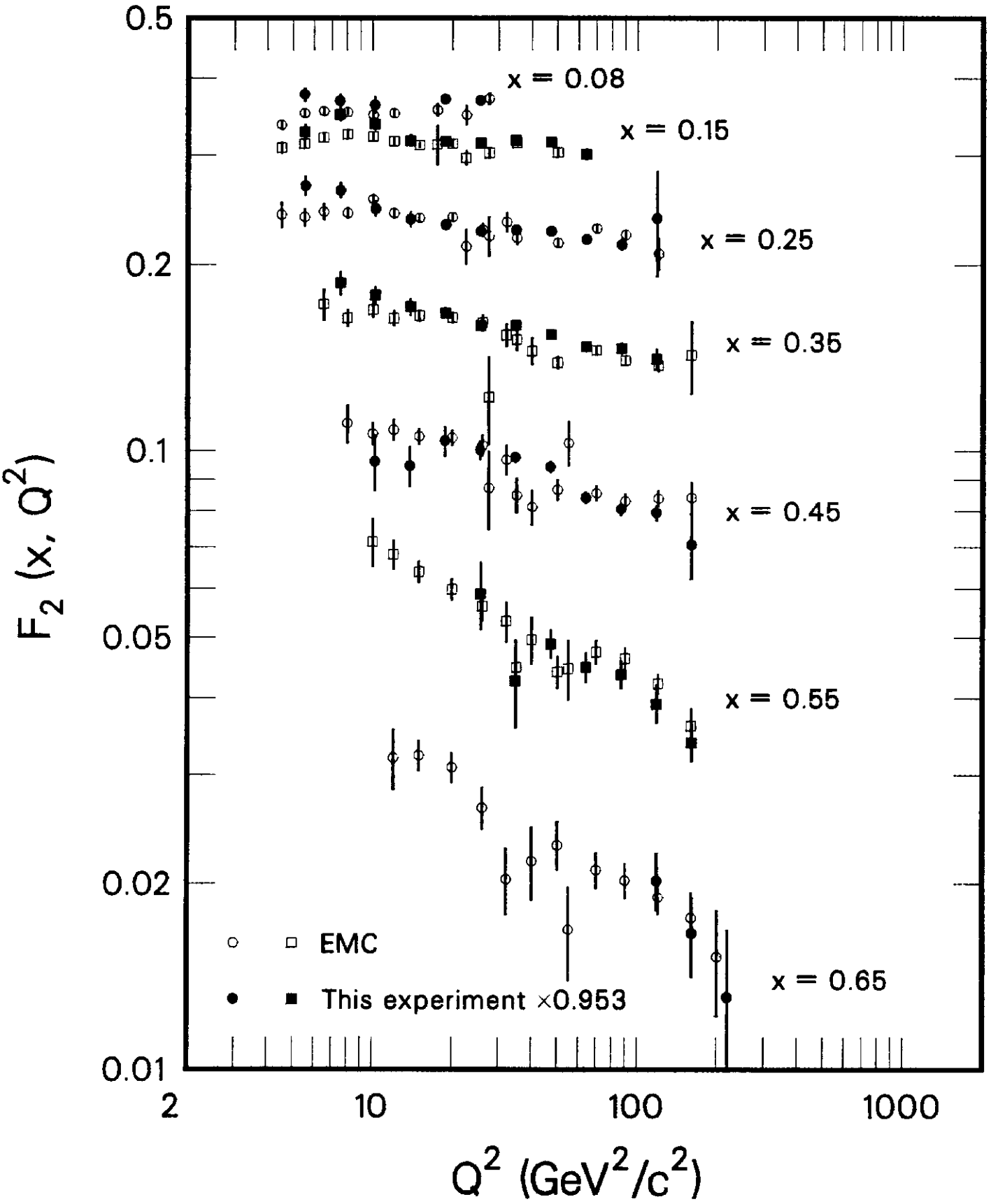
0.5
0.2
0.1
0.05
0.02
0.01
2
10
100
1000
$F_2(x, Q^2)$
Q^2 (GeV^2/c^2)
x = 0.08
x = 0.15
x = 0.25
x = 0.35
x = 0.45
x = 0.55
x = 0.65
EMC
This experiment ×0.953
XCG 836-7167

FIGURE 4.

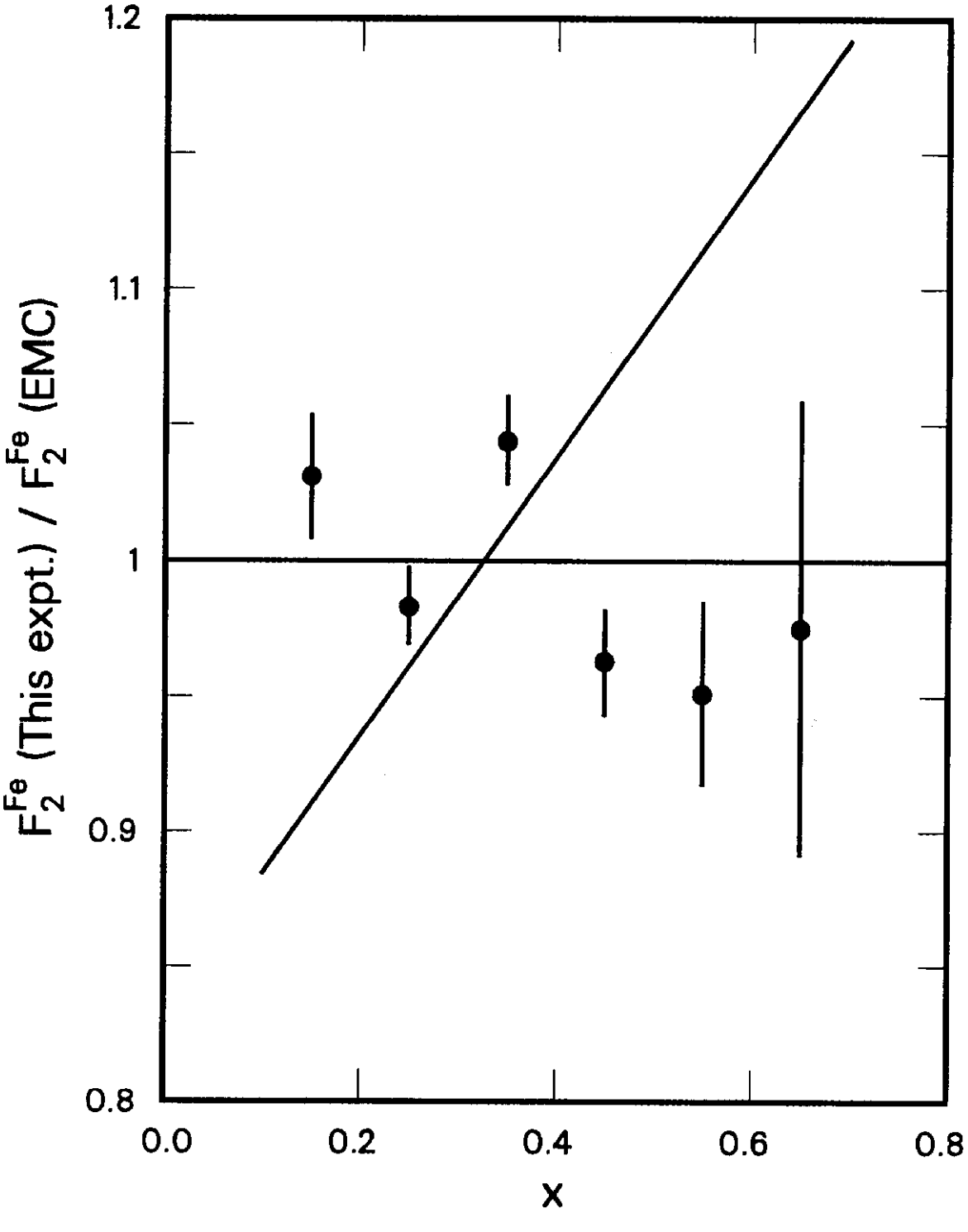

FIGURE 5.